

Encounter rate by turbulent shear of particles similar in diameter to the Kolmogorov scale

by P. S. Hill,^{1,2} A. R. M. Nowell¹ and P. A. Jumars¹

ABSTRACT

To clarify the rate at which particles similar in size to the smallest eddies in a turbulent fluid encounter one another via turbulent shear, 3-D video motion analysis was used to make direct measurements of relative velocities between closely spaced, near-neutrally buoyant, 700- μm mean diameter, polystyrene latex spheres suspended in an oscillating-grid turbulence tank. Smallest eddy size, termed the Kolmogorov scale, λ , was estimated as $(\nu^3/\epsilon)^{0.25}$ where ν is fluid viscosity and ϵ is the dissipation rate of turbulent kinetic energy. For runs made in water, the effective particle diameter examined was ≈ 3 –6 times larger than λ . To measure relative velocities for particles just smaller than the Kolmogorov scale, the viscosity of the suspending fluid was increased ≈ 25 times by the addition of Methocel, a commercially available, methyl cellulose synthetic gum used for fluid thickening. For runs made in Methocel, effective sphere diameter was ≈ 0.2 –0.5 times the Kolmogorov scale. Turbulent kinetic energy dissipation rate was estimated by traversing the measuring volume of a laser-Doppler velocimeter fiberoptic probe through the fluid at speeds high relative to the fluctuating fluid velocities in the tank. Resulting time series were used in analogy with instantaneous spatial series to calculate root-mean-square fluctuating velocities and integral length scales of turbulence, which in turn served as input for calculation of ϵ . By examining the relationship between Reynolds number based on relative velocity between particles and particle separation distance relative to λ , two competing hypotheses were tested. The first, that turbulent eddying motions control relative velocity between closely spaced particles, was accepted for particles both slightly larger and slightly smaller than the Kolmogorov scale ($0.05 < p < 0.10$). The second, that viscous forces control relative velocity between particles, was strongly rejected in both cases ($p = 0.004$). The finding contradicts earlier assumptions and assertions that viscosity dominates small-scale particle interactions for sizes near the Kolmogorov scale, and it indicates that relative velocities between particles are greater than previously thought. Relative to biological mechanisms of particle encounter, turbulence therefore plays a role greater than is presently assumed in effecting encounter among particles and also between particles and organisms.

1. Introduction

Particle encounter induced by small-scale turbulence plays several hypothetical roles in the marine environment. By repackaging small, slowly sinking particles into

1. School of Oceanography, WB-10, University of Washington, Seattle, Washington, 98195, U.S.A.

2. Present address: Department of Oceanography, Dalhousie University, Halifax, Nova Scotia, B3H 4J1, Canada.

large, rapidly sinking ones, physical aggregation presumably enhances open-ocean vertical fluxes of adsorbed chemical species (e.g., Bacon *et al.*, 1985), fine lithogenic and biogenic material (e.g., Honjo, 1982), and phytoplankton biomass following blooms (e.g., Smetacek, 1985; Hill, 1992). In the nearshore, physical aggregation by turbulent shear provides a mechanism for trapping fine sediment and particle-associated pollutants in estuaries and other coastal environments (e.g., van Leussen, 1988). Encounter rates between predator and prey may show substantial increases due to turbulence-induced relative motion (Rothschild and Osborn, 1988). Lastly, rate of access of phytoplankton and bacteria to small-scale nutrient patches in an oligotrophic environment may be governed by turbulent motion at small scales (Rothschild and Osborn, 1988). Efforts to predict vertical fluxes and predator-prey encounter rates and to understand nutrient cycling in rarefied environments therefore depend upon knowledge of turbulence-induced particle encounter rates.

Smoluchowski (1917) first proposed kinetic equations to describe the rate of change in total particle concentration due to aggregation. For a dilute, monodisperse suspension the initial rate of change in total particle concentration is (Smoluchowski, 1917):

$$\frac{dN}{dt} = -KN^2, \quad (1)$$

where N is total particle number density (cm^{-3}), and K is a second order encounter-rate coefficient ($\text{cm}^3 \text{s}^{-1}$). In theory the rate coefficient describing particle encounter due to turbulent shear takes varying form depending on particle size relative to the smallest eddies in the fluid. Smallest eddy size in the fluid, termed the Kolmogorov scale, λ , is defined as $(\nu^3/\epsilon)^{0.25}$, where ν is kinematic viscosity ($\text{cm}^2 \text{s}^{-1}$), and ϵ is the turbulent kinetic energy dissipation rate ($\text{cm}^2 \text{s}^{-3}$) (cf. Tennekes and Lumley, 1972). Oceanic dissipation rates span many orders of magnitude from 10^{-6} to $10^2 \text{ cm}^2 \text{ s}^{-3}$ (Yamazaki and Osborn, 1988). Therefore minimal eddy size indicated by this calculation may be as large as 1 cm or as small as 10^{-2} cm. Marine particle sizes range from sub-micrometer to meter scales (e.g., Sheldon *et al.*, 1972), indicating the importance of encounter-rate expressions for particles both smaller and larger than the Kolmogorov scale.

Expressions for the encounter-rate coefficient, K , of particles much smaller and much larger than the Kolmogorov scale have been proposed (Saffman and Turner, 1956; Delichatsios and Probst, 1975). Theory for encounter rate of particles similar in size to the Kolmogorov scale does not exist, leaving a critical gap in the ability to predict particle encounter rates in the ocean. For example, in the upper mixed layer, where dissipation rates typically range between 10^{-4} to $10^{-2} \text{ cm}^2 \text{ s}^{-3}$ (Veth, 1983), λ is of order 0.1 cm. Therefore, encounter rates of particles in the dynamically significant range of 0.01–1 cm in size are poorly constrained. It is the objective of this study to fill this gap in understanding by making the first direct

observations in a controlled laboratory environment of the encounter rates of particles slightly smaller and slightly larger than the Kolmogorov scale.

2. Theory

Encounter-rate expressions used here are derived under a shared set of assumptions. These assumptions are: particle inertia is small so that particles follow the flow; turbulence is isotropic; particle-particle interactions are negligible; and gravitational forces are negligible (Saffman and Turner, 1956; Delichatsios and Probstein, 1975). Under these assumptions, the encounter-rate coefficient, K (Eq. 1), equates with the volume swept out by a particle per unit of time. Considering spheres of one size, the encounter-rate coefficient may be expressed as:

$$K = \pi d^2 u_r, \quad (2)$$

where d is distance between centers of two touching spheres and u_r is the relative velocity between colliding particles (cf. Delichatsios and Probstein, 1975).

The relative particle velocity, u_r (Eq. 2), has been assumed approximately equal to the root-mean-square relative turbulent velocity between two points at a distance d apart (Delichatsios and Probstein, 1975). Implicit in this assumption are the notions that particles are passive tracers of fluid motion and that the fact that particles are finite and nondeformable does not alter particle-particle relative velocities. By drawing on Kolmogorov theory for isotropic turbulence (e.g., Tennekes and Lumley, 1972), Delichatsios and Probstein (1975) hypothesized that relative velocity, u_r , is defined as:

$$u_r = 0.26(\epsilon/\nu)^{1/2}d \quad (3)$$

for particles smaller than the Kolmogorov scale and:

$$u_r = 1.37(\epsilon d)^{1/3} \quad (4)$$

for particles larger than the Kolmogorov scale. Saffman and Turner (1956) employed a more elaborate calculation to arrive at an expression for sub-Kolmogorov-scale relative velocity that differs from Eq. 3 only in the leading coefficient. The expression is:

$$u_r = 0.10(\epsilon/\nu)^{1/2}d \quad (5)$$

Eq. 5 is more commonly used than Eq. 3. The forms of sub- and super-Kolmogorov-scale expressions arise from dimensional considerations. In the former viscosity plays a strong role in determining u_r , whereas in the latter viscosity is irrelevant.

The discussion of how relative velocity varies with dissipation rate, viscosity and particle separation simplifies substantially by multiplying Eqs. 3–5 by the ratio of particle separation to viscosity. The resulting non-dimensional equations express a

relative-velocity-based Reynolds number as a function of the ratio of particle separation to Kolmogorov scale. The sub-Kolmogorov-scale expression (Eq. 5), may be rewritten as:

$$Re = 0.10(d/\lambda)^2 \quad (6)$$

where Re is Reynolds number ($= u_r d/\nu$) (The leading coefficient equals 0.26 if one follows Eq. 3.) The super-Kolmogorov-scale expression (Eq. 4) becomes:

$$Re = 1.37(d/\lambda)^{4/3}. \quad (7)$$

Inspection reveals that Eqs. 6–7 do not match as they should when d equals λ .

Two competing hypotheses for relating Re to (d/λ) when $0.1 \leq (d/\lambda) \leq 10$ may be erected. First, one can assume that viscous forces control the relative velocity between two points in this dynamical region, and relative-velocity Reynolds number, therefore, is defined by Eq. 6. This hypothesis receives implicit acceptance when a unified expression for the Reynolds number is formed by matching Eqs. 6–7 and assuming that Eq. 6 holds below the matching size and Eq. 7 holds above this size (Delichatsios and Probstein, 1975; Hill, 1992). It finds support in studies that show a rapid fall off in turbulent shear energy at scales less than roughly ten times the Kolmogorov scale (e.g., Grant *et al.*, 1962; Oakey and Elliott, 1980). Second, one can assume that fluid inertia controls relative velocity between two points separated by a distance roughly equal to the Kolmogorov scale. In this case Reynolds number is defined by Eq. 7. This hypothesis finds support in theoretical work suggesting that particles similar in diameter to the Kolmogorov scale respond only to fluid motions at scales larger than the Kolmogorov scale (Hinze, 1972).

3. Methods

a. Materials. Parameters that must be measured are relative velocity between closely spaced particles, separation distance between particles, kinematic viscosity and the dissipation rate of turbulent kinetic energy (e.g., Eq. 4–5). The statistical formulation of theory for relative velocity between particles demands that a relatively large sample be used to provide an adequate test. This requirement suggested the use of 3-D video motion analysis because of its capacity to process large amounts of video data rapidly. Particles were tracked in three dimensions through time with a system built by Motion Analysis Corporation. As used, the system comprised two NEC TI 22PII CCD video cameras equipped with Tamron 1 : 2.5, 90 mm, Tele-Macro lenses, a Motion Analysis Corporation VP-310 video processor and a Sun Microsystems 3/160 workstation equipped with Motion Analysis Expertvision software.

Particles were tracked in an oscillating-grid turbulence tank. The square, plexi-glass tank measured $50 \times 50 \times 40$ cm. A grid of aluminum bars, 1-cm square in cross section, spaced 6.35 cm between centers, was driven by a Bodine DC, adjustable-speed gear motor. The motor drove a wheel connected to a center post, that in turn

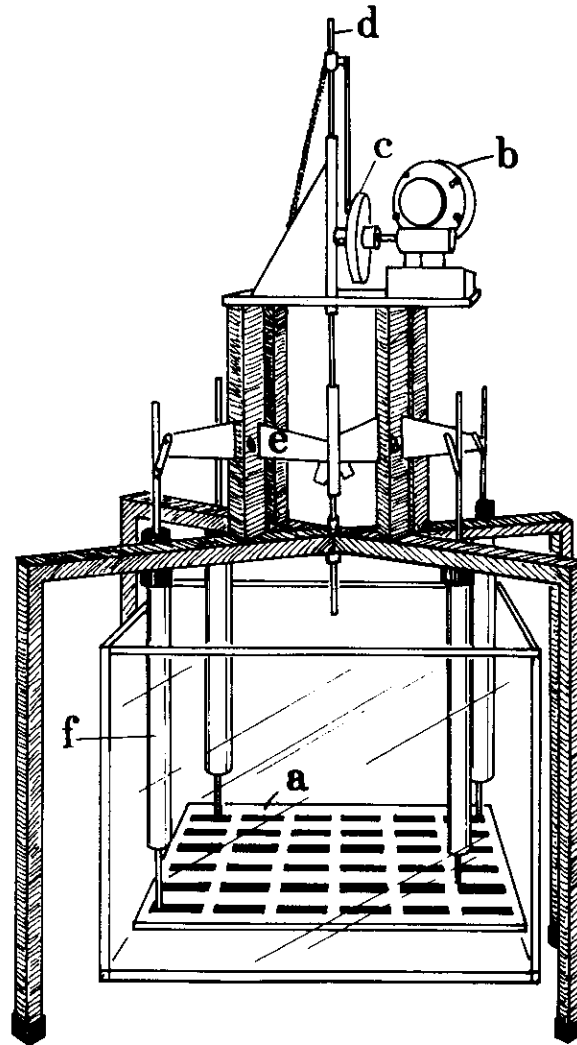


Figure 1. Schematic of oscillating-grid turbulence tank. The tank measures $50 \times 50 \times 40$ cm (wide, long and tall, respectively). The grid of aluminum bars (a) is driven by a DC, adjustable-speed gear motor (b). The motor drives a wheel (c) connected to a center post (d) that pumps four levers (e). The levers link to stainless steel, sleeved legs (f) that attach to the grid.

pumped four levers attached to stainless steel, sleeved legs. The legs were affixed to the grid (Fig. 1). Turbulent kinetic energy dissipation rate in the tank is a function of grid-stroke amplitude, grid-stroke frequency, and distance from the grid (Brumley and Jirka, 1987). Amplitude was adjusted by moving the wheel attachment point of the linkage between wheel and center post. Frequency was adjusted with motor

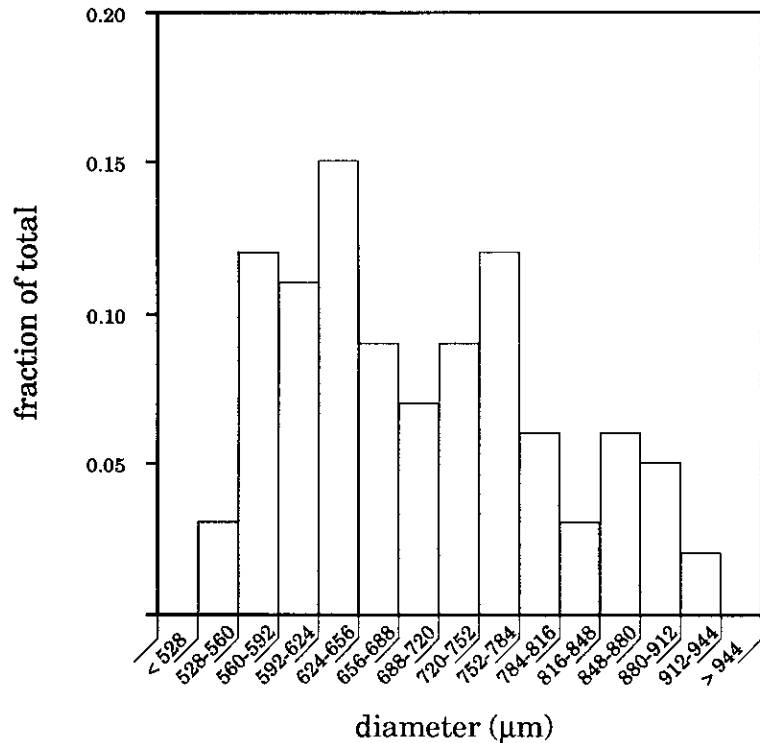


Figure 2. Size-frequency distribution of polystyrene latex spheres, based on microscopic measurement of 100 particles. Mean diameter is 0.070 cm; median diameter is 0.067 cm.

speed. Depth of measurements stayed constant at 28.5 cm above the tank bottom (20.5 cm above the grid-stroke midpoint) throughout the experiment. Aside from the drive mechanism, the tank matches closely in design the tank in which detailed turbulence measurements were made by Brumley and Jirka (1987). At 28.5 cm above the tank floor, turbulence is approximately isotropic (Brumley and Jirka, 1987).

Dark blue, opaque, polystyrene latex spheres with a density of 1.035 g cm^{-3} were tracked. Mean particle size, as estimated from microscopic measurements of 100 particles, was $700 \text{ } \mu\text{m}$ (Fig. 2). High contrast between particles and background, which is essential for effective tracking, was achieved by backlighting sheets of white acrylic taped to the tank faces directly opposite the faces of the tank into which the cameras pointed. To reduce the amount of stray light in the tank, black poster board was taped to all sides. Only windows around the white acrylic and the cameras were left open.

Two cameras were positioned to look into the tank through orthogonal faces. Lens faces were roughly 30 cm from the tank. Camera positions had to be carefully calibrated in order for the motion analytic software to be successful in tracking particles. Calibration is performed by placing as few as 6 or as many as 30 objects in

Table 1. Chemical composition and physical properties of suspending fluids. Concentrations of NaCl and Methocel are given in mass per unit of volume (g cm^{-3}). Other parameters are fluid density, ρ (g cm^{-3}), fluid temperature, T ($^{\circ}\text{C}$), kinematic viscosity, ν ($\text{cm}^2 \text{s}^{-1}$), and water depth, h (cm).

	NaCl	Methocel	ρ	T	ν	h
water	0.056	0.000	1.035	18	0.012	35.5
Methocel solution	0.056	0.005	1.035	21	0.300	35.5

the viewing fields of both cameras. The positions of the objects relative to one another ideally are known to within one-one thousandth of the viewing width. The viewing field measured 2.54 cm on a side. The calibration object consisted of eighteen insect pins implanted to varying depths in black plastic. The positions of the light-colored pinheads, which contrasted with the dark stems, were measured on a mill table. Two sighting scopes allowed precise alignment on the pinheads. Positions were measured three times to within 0.00254 cm.

The dissipation rate of turbulent kinetic energy may be estimated as:

$$\epsilon = A \frac{u'^3}{l} \quad (8)$$

where A is a constant near unity, u' is the root-mean-square fluctuating velocity and l is the integral length scale of the turbulence (cf. Tennekes and Lumley, 1972). This scale is calculated as the area under the curve generated by plotting spatial autocovariance of velocity as a function of spatial separation. In a fluid with zero mean flow, one may make analogy between an instantaneous spatial series and a time series generated by moving a flow meter fast relative to the fluctuating velocities in the fluid (Tennekes and Lumley, 1972). Time series of velocity were sampled by a TSI laser-Doppler velocimeter fiberoptic probe system. The system was powered by a Lexel Model 85, 1-Watt, argon-ion laser. The probe measured 2.54 cm in diameter, and had a focal distance of 10.0 cm in air. The measuring volume was 12 cm from the wall in all runs. The signal was processed with a TSI Model 1980 counter-type signal processor. The processor was operated in total burst mode, and mean velocity for a burst was calculated by averaging point estimates of velocity obtained from eight burst cycles. A frequency shift of 50 kHz was applied to one of the outgoing beams by a TSI Model 9182 Bragg cell so that probe direction could be discerned. The probe was traversed back and forth parallel to the outside of the tank wall at a speed of 9.83 cm s^{-1} . Only the velocity parallel to the direction of traverse was measured. Data were transmitted to a Zenith PC by a TSI MI-990 Interface, where data were reduced and stored by TSI FIND software. Data included velocity and time between bursts. The signal was enhanced by seeding the fluid with TSI-supplied, 4- μm diameter, metal-coated spheres with a density of 2.6 g cm^{-3} .

The probe traverser consisted of a probe support joined to two pivoting linkages

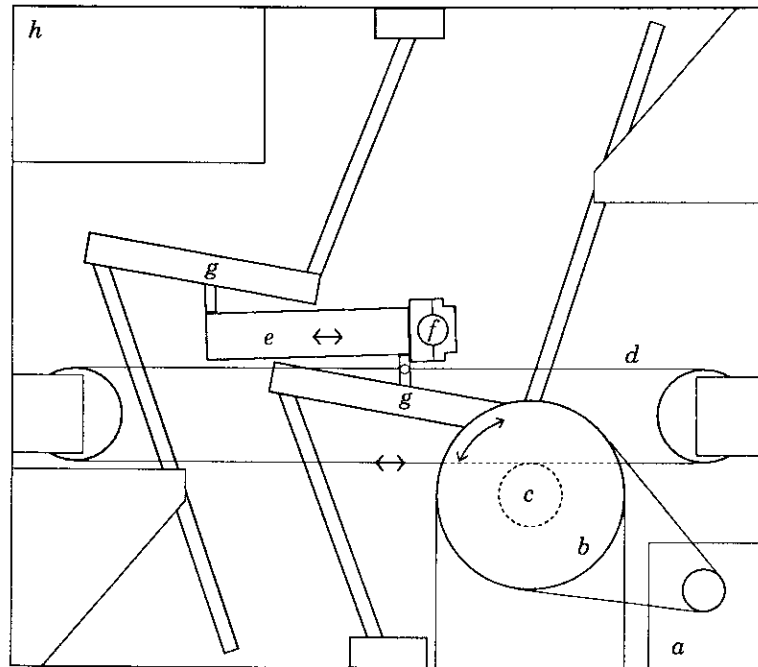


Figure 3. Schematic of LDV fiberoptic probe traverser. The traverser is driven by a reversible, synchronous, permanent magnet-type instrument motor (a) equipped with an integral friction clutch. The motor turns a 3.5-cm-diameter pulley, that drives an O-ring belt attached to a 15-cm-diameter pulley (b). The larger pulley is attached to a rotating drum (c), around which wraps a thin wire (d). The wire drives the probe support apparatus, which comprises the support (e), the probe clamp (f), and two pivoting linkages (g). Electronics (h) are housed in the upper left-hand corner of the unit.

that forced linear horizontal motion with insignificant sigmoidal vertical motion. The probe support was driven by a thin steel wire that wrapped around a drum. The drum was rotated by a 15-cm diameter pulley driven by an O-ring belt attached to a 3.5-cm diameter pulley. The 3.5-cm pulley was driven by a reversible, synchronous, permanent-magnet-type instrument motor equipped with an integral friction clutch. The clutch smoothed the probe velocity during reversal of motion. The motor ran at 300 RPM (Fig. 3). The length of the traverse was 20 cm. The beginning of each forward and backward traverse was signalled by a 1- μ s ttl sync pulse sent by the traverser to the MI-990 interface. The time of occurrence of each pulse was recorded with other data.

The size of particles relative to the Kolmogorov scale was altered by manipulating fluid viscosity. An aqueous 5.6% NaCl solution (density = 1.035 g cm⁻³) was used for runs in which particle size was to be larger than the Kolmogorov scale. A 0.5% solution of Dow Chemical J5MS Methocel and 5.6% NaCl water was used for runs in which particles were to be smaller than the Kolmogorov scale. Low-concentration

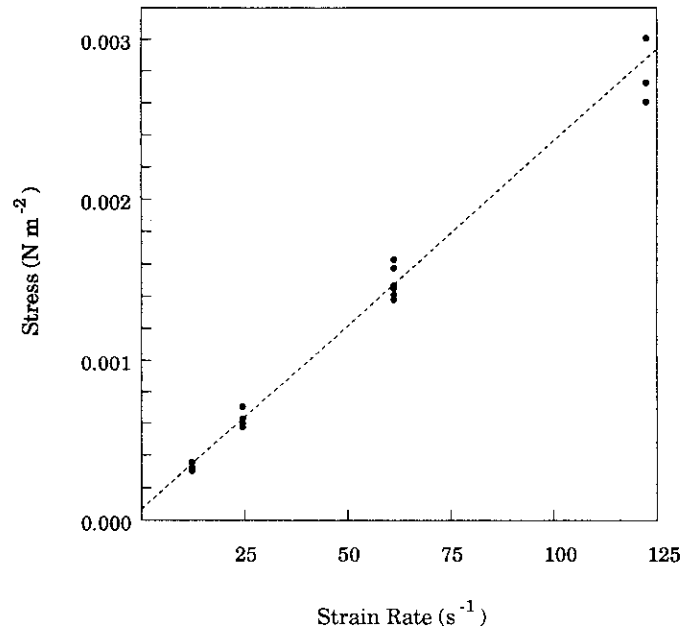


Figure 4. Stress (N m^{-2}) versus strain rate (s^{-1}) for a 0.5% aqueous solution of Dow Chemical J5MS Methocel. Dotted line is linear best fit: (slope = 2.24×10^{-4} ; intercept = 6.68×10^{-5}).

Methocel solutions as used here show Newtonian viscosity (Fig. 4). Viscosity was monitored throughout experiments with Methocel with a Brookfield Model TA-II viscometer equipped with a UL concentric-cylinder spindle adapter. A 0.5% Methocel solution has a kinematic viscosity of roughly $0.3 \text{ cm}^2 \text{ s}^{-1}$ (Table 1).

b. Experimental design and procedures. The experiment was divided into two parts. One set of measurements was made in the solution of NaCl and water, and the other set was made in the high-viscosity Methocel and NaCl solution. Video data could not be taken contemporaneously with LDV data due to space constraints on placement of equipment around the tank.

The video motion analysis measurements for each fluid viscosity were carried out in two randomized blocks. Blocks were differentiated by location in the tank. Each block comprised nine treatments. Each treatment was a combination of one of three grid-stroke amplitudes and one of three grid-stroke frequencies. Treatment order was randomized within each block.

Within a given treatment 10 observations were made. Each observation consisted of 90 frames of video data. The time over which the 90 frames of data were gathered varied between the high- and low-viscosity runs. Frame rate for data collection was chosen so that the rate of capture exceeded the highest expected turbulent frequencies in the tank. These frequencies may be calculated as $(\epsilon/\nu)^{1/2}$ (e.g., Tennekes and

Lumley, 1972). Maximal dissipation rates were of order unity for both viscosities, yielding maximal frequencies of $\approx 10 \text{ s}^{-1}$ for the aqueous NaCl solution and of $\approx 2 \text{ s}^{-1}$ for the Methocel solution. Frame rates of 30 and 10 s^{-1} were deemed adequate for capturing the highest-frequency turbulent fluctuations in the low- and high-viscosity blocks, respectively. Therefore, duration of capture for a given observation was 3 s for the low- and 9 s for the high-viscosity runs.

For each treatment, the calibration object was placed in the appropriate location in the tank. The two cameras were positioned such that the calibration object control points (the heads of the insect pins) filled the viewing area of each camera. The calibration object was removed. The grid was turned on at the amplitude and frequency designated for that treatment. The cameras and the video processor were adjusted to maximize data quality (primarily a function of contrast and gray level threshold on the video processor). Fluid temperature was measured and recorded. Fluid density was measured by hydrometer and recorded. For runs with Methocel, fluid viscosity was measured with a Brookfield viscometer. The calibration object was repositioned and calibration video files were collected. The calibration object was removed, and great care was taken not to bump either the cameras or the tank. The grid was started and allowed to run for a minimum of 600 s prior to gathering data. Observation times were separated by random intervals calculated by adding the mean overturn time in the tank (approximated as 50 s) to a random number (between 0 and 1) times the mean overturn time.

Procedures for gathering flow data with the LDV proceeded similarly, although only one block of data was gathered for each viscosity. Treatment order was randomized within blocks. For each treatment the grid was turned on at the appropriate amplitude and frequency. Fluid temperature and density were measured. The grid was allowed to run for a minimum of 600 s before measurements were made. Three observations were made for each treatment. Each observation consisted of 30 s of velocity data. Sample rates were of order $100 \text{ bursts s}^{-1}$. The interval between LDV observations was set identically to the interval between video observations.

c. Data reduction and analysis. Motion Analysis Corporation Expertvision software was used to produce particle track data. Camera positions were calibrated for each treatment. The track operator in the software assigns a unique path number to each particle tracked, and it provides frame number, time from start and x, y, and z coordinates as a function of frame. Data files were translated to ASCII format for further processing.

Reduction of track data involved identifying closely spaced particles and measuring relative velocity between them. Definition of "closely spaced" was operational, and was constrained by dynamical considerations. Theory for relative velocity between closely spaced particles was formulated under the assumptions of negligible

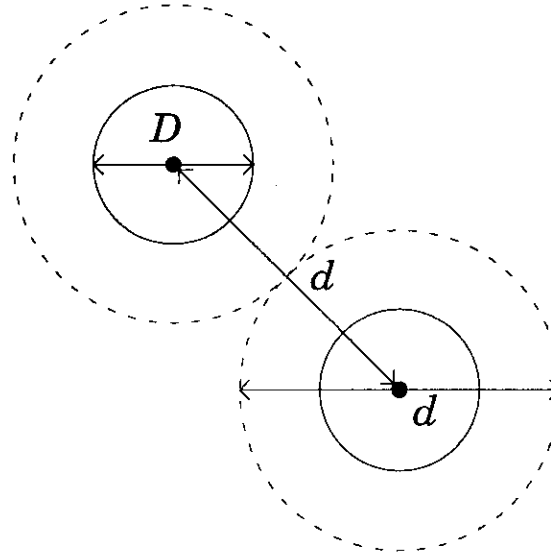


Figure 5. Relationship of particle diameter, D , to particle separation distance and analogous particle diameter, d . In this case $d = 2D$, so that by measuring relative velocity between spheres with centers separated by d encounter rate between spheres twice the diameter of the actual spheres is being used.

particle-fluid and particle-particle interactions (Saffman and Turner, 1956; Delichatsios and Probst, 1975). The first assumption of negligible particle-fluid interaction reduces the problem to one of estimating relative velocity between the two fluid points that would be located at the spheres' centers in the absence of the spheres. The second assumption of negligible particle-particle interaction requires that relative velocities be estimated from particles that are separated by a distance sufficient to make interaction effects on relative velocities small. Assuming uniform straining motion on the scale of particles, velocity disturbance caused by a sphere increases rapidly for distances smaller than two diameters from the sphere center (e.g., Landau and Lifschitz, 1959). Therefore, analysis focused on particles with centers separated by two to three diameters. This range imposed maximal velocity disturbances of $< 20\%$. The mean disturbance was substantially less, because separations were biased to higher values by the spherical geometry of the problem (i.e., there being much more fluid volume at three-diameter separation than at two). The upper limit to separation restricts the spread in measured relative velocities. By focusing on spheres separated by two to three diameters, analogy is made, in terms of theory, with spheres two to three times the diameter of the actual spheres (Fig. 5). Again, this analogy rests on the assumption that particle-particle relative velocity equals fluid-fluid relative velocity. Encounter-rate theory makes no distinction between the relative velocities between two solid spheres of diameter $2d$ in contact, two fluid spheres of diameter $2d$ in contact, or as in the present case, two solid

Table 2. Values for median relative-velocity Reynolds number ($u, \bar{d}/\nu$) and mean distance of separation between centers of interacting spheres, \bar{d} (cm), as a function of treatment number in runs in water. Numbers in parentheses represent one standard deviation.

Treatment	Re	\bar{d}
1	2.941	0.198 (0.011)
2	3.282	0.179 (0.022)
3	4.264	0.190 (0.021)
4	3.570	0.187 (0.019)
5	4.087	0.190 (0.021)
6	5.530	0.190 (0.018)
7	3.683	0.187 (0.021)
8	4.734	0.188 (0.017)
9	5.892	0.192 (0.014)

spheres of diameter d with centers $2d$ apart circumscribed by fluid shells of thickness $d/2$ (Fig. 5).

Upon identifying two particles with centers separated by between two and three particle diameters, the previous frame was searched for the same two particles. If located, relative velocity was calculated as the product of change in separation and the frame rate. Failure to locate particles in the preceding frame initiated a search in the succeeding frame. If found, relative velocity was calculated identically. Separation was measured from the first frame in which the particle separation was less than three diameters. The relative velocity Reynolds number was then calculated by dividing the product of relative velocity and separation by kinematic viscosity.

The first step in the analysis of the Reynolds number data was to ask whether measurements made in two different tank locations could have been sampled from the same parent population. Because the underlying distribution of relative-velocity Reynolds number is unknown, the two-sample Kolmogorov-Smirnov test (Conover, 1980) was applied to the data from each treatment. In 17 of 18 cases, at an α level of 0.05, the data could be considered to derive from the same underlying distribution.

Table 3. Values for median relative-velocity Reynolds number ($u, \bar{d}/\nu$) and mean distance of separation between centers of interacting spheres, \bar{d} (cm), as a function of treatment number in runs in Methocel solution. Numbers in parentheses represent one standard deviation.

Treatment	Re	\bar{d}
1	0.182	0.173 (0.022)
2	0.204	0.194 (0.015)
3	0.248	0.191 (0.015)
4	0.193	0.189 (0.018)
5	0.241	0.187 (0.023)
6	0.292	0.186 (0.028)
7	0.224	0.188 (0.018)
8	0.279	0.186 (0.025)
9	0.465	0.188 (0.021)

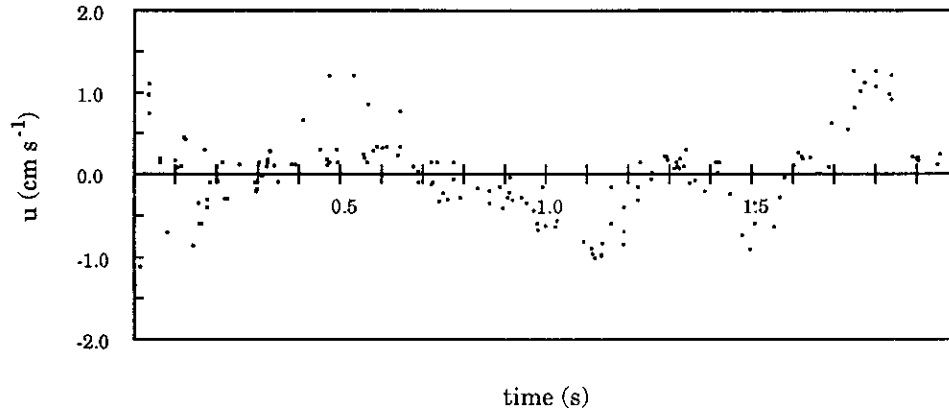


Figure 6. Typical trace of velocity (mean subtracted) measured with the LDV as a function of time after a ttl pulse. Traverse is from treatment 7 in water. Sample size is 167.

typically with p values greater than 0.2. Therefore, the two low-viscosity blocks were grouped, as were the two high-viscosity blocks.

Next, the possibility that values of Re in the experiment were normally or lognormally distributed was explored. Using the Shapiro-Wilk test for normality (Conover, 1980), the null hypotheses of normality and lognormality both were strongly rejected ($p < 0.01$) at an α level of 0.05. The remainder of the analysis, therefore, was conducted nonparametrically, and median values of Re were used in further calculations (Tables 2, 3).

To produce estimates of fluctuating velocities in the tank required that the data be rotated and the mean, subtracted. Because it was not possible to position the probe precisely so that the axis of the two beams lay parallel to the tank grid, data for each treatment were rotated. Optimal rotation yielded a best fit between the sample mean velocity and the mean velocity of the probe traverser. To remove any unsteadiness in probe velocity associated with direction reversals, only data points gathered between 0.5–1.5 s after a ttl pulse were analyzed. After rotation, the mean was subtracted (Fig. 6).

Root-mean-square velocity and integral length scale used in calculating turbulent kinetic energy dissipation rate (Eq. 8) were estimated with the mean discrete temporal velocity autocorrelation function $R(k)$ (Fig. 7). Values of $R(k)$ were calculated as:

$$R(k) = \frac{1}{N_k} \sum u(t)u(t + k\Delta\tau), \quad (9)$$

where N_k is number of observations at lag $k\Delta\tau$, $u(t)$ is the velocity at time t , $u(t + k\Delta\tau)$ is the velocity at time $(t + k\Delta\tau)$, k is bin number and $\Delta\tau$ is bin size. Because the data were randomly spaced in time, calculation of $R(k)$ was preceded by binning the data (Smith and Meadows, 1974). For each observation the middle eight traverses were

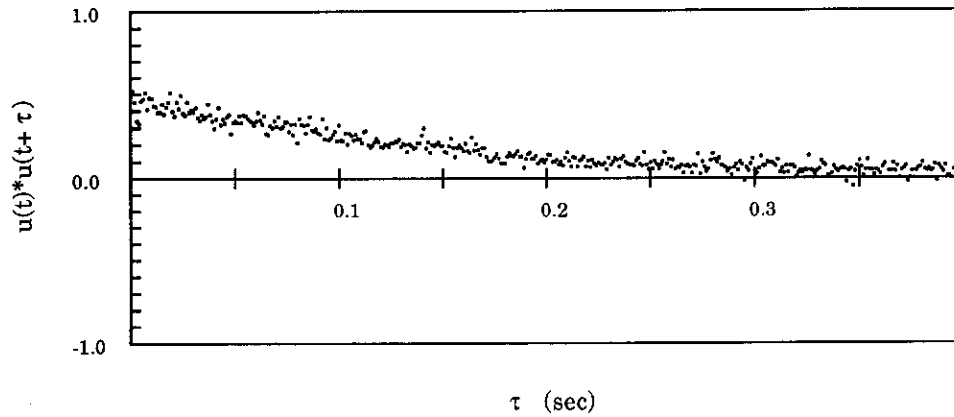


Figure 7. Typical discrete, temporal, velocity autocorrelation out to a lag of 0.4 s with a 0.001-s bin size. Autocorrelation is the composite from all traverses for treatment 7 in water.

grouped to generate estimates of the autocorrelation function. Estimates of $R(k)$ from the three observations in each treatment were averaged to yield one value for $R(k)$ for each lag for each treatment. A bin size of 10^{-3} s and a bin number of 400 were selected.

Dissipation rate was calculated with Eq. 8 assuming a value for A of unity. Fluctuating root-mean-square velocity u' was estimated as the square root of the velocity autocorrelation function at lag zero. The integral length scale was estimated from the area under the autocorrelation curve normalized by autocorrelation at zero lag, $R(0)$. The equation is:

$$l = \frac{U\Delta t}{R(0)} \sum_{k=0}^{399} R(k). \quad (10)$$

The standard deviation in ϵ , denoted as σ_{ϵ} , was estimated by propagating errors

Table 4. Grid-stroke frequency, f (s^{-1}), grid-stroke amplitude, S (cm), estimated root-mean-square fluctuating velocity, u' ($cm\ s^{-1}$), integral length scale, l (cm), turbulent kinetic energy dissipation rate, ϵ , and Kolmogorov scale, λ , for each treatment for runs made in water. Numbers in parentheses represent one standard deviation.

Treatment	f	S	u'	l	ϵ	λ
1	2.5	4.0	0.429 (0.004)	1.033 (0.059)	0.076 (0.006)	0.069 (0.003)
2	2.5	5.0	0.649 (0.005)	1.430 (0.062)	0.191 (0.013)	0.055 (0.002)
3	2.5	6.0	0.782 (0.006)	1.108 (0.058)	0.441 (0.033)	0.045 (0.002)
4	3.0	4.0	0.600 (0.005)	1.064 (0.063)	0.204 (0.018)	0.054 (0.002)
5	3.0	5.0	0.791 (0.007)	1.372 (0.065)	0.360 (0.026)	0.047 (0.002)
6	3.0	6.0	1.021 (0.009)	0.954 (0.059)	1.115 (0.097)	0.035 (0.002)
7	3.4	4.0	0.696 (0.007)	1.332 (0.066)	0.253 (0.021)	0.051 (0.002)
8	3.4	5.0	0.894 (0.008)	1.103 (0.061)	0.648 (0.052)	0.040 (0.002)
9	3.4	6.0	1.250 (0.009)	1.298 (0.058)	1.504 (0.100)	0.033 (0.001)

Table 5. Grid-stroke frequency, f (s^{-1}), grid-stroke amplitude, S (cm), estimated root-mean-square fluctuating velocity, u' ($cm\ s^{-1}$), integral length scale, l (cm), turbulent kinetic energy dissipation rate, ϵ , and Kolmogorov scale, λ (cm), for each treatment for runs made in Methocel solution. Numbers in parentheses represent one standard deviation.

Treatment	f	S	u'	l	ϵ	λ
1	2.5	4.0	0.332 (0.003)	1.307 (0.068)	0.028 (0.002)	0.992 (0.041)
2	2.5	5.0	0.392 (0.004)	1.729 (0.068)	0.035 (0.003)	0.938 (0.031)
3	2.5	6.0	0.436 (0.004)	1.280 (0.062)	0.065 (0.005)	0.803 (0.032)
4	3.0	4.0	0.394 (0.004)	2.065 (0.078)	0.030 (0.002)	0.976 (0.032)
5	3.0	5.0	0.505 (0.005)	1.735 (0.069)	0.074 (0.005)	0.777 (0.026)
6	3.0	6.0	0.643 (0.006)	1.676 (0.064)	0.158 (0.010)	0.642 (0.021)
7	3.4	4.0	0.482 (0.004)	1.970 (0.079)	0.057 (0.003)	0.831 (0.027)
8	3.4	5.0	0.612 (0.005)	1.755 (0.066)	0.130 (0.008)	0.674 (0.022)
9	3.4	6.0	1.141 (0.008)	1.675 (0.054)	0.886 (0.046)	0.418 (0.011)

incurred in estimating $R(0)$ and l . A summary of error-propagation methodology used here appears in Taylor (1982). The formula for estimating the standard deviation of ϵ had the final form:

$$\sigma_{\epsilon} = \epsilon \left(2.5 \frac{\sigma_{R(0)}}{R(0)} + \frac{U\Delta\tau}{lR(0)} \sum_{k=0}^{399} \sigma_{R(k)} \right). \quad (11)$$

In the equation $\sigma_{R(0)}$ is the standard deviation in estimates of $R(0)$ and $\sigma_{R(k)}$ is the standard deviation in estimates of $R(k)$. Measured dissipation rates in the water runs compared well with dissipation rates based on predicted values of u' and l (Brumley and Jirka, 1987) (Fig. 8; Table 4). Dissipation rates in the tank showed grid Reynolds number sensitivity as evidenced by lower measured dissipation rates in the Methocel runs (Table 5).

The ratio of mean separation distance, \bar{d} , to Kolmogorov scale, λ , was calculated as:

$$\frac{\bar{d}}{\lambda} = \bar{d} \left(\frac{\epsilon}{\nu^3} \right)^{1/4}. \quad (12)$$

The standard deviation in estimates of (\bar{d}/λ) , $\sigma_{(d/\lambda)}$, was calculated as (Taylor, 1982);

$$\sigma_{(d/\lambda)} = \frac{\sigma_d}{\lambda} + \frac{\bar{d}\sigma_{\lambda}}{\lambda^2}, \quad (13)$$

where σ_d is the standard deviation in measurements of separation and σ_{λ} is the standard deviation in estimates of the Kolmogorov scale. The latter is calculated as:

$$\sigma_{\lambda} = \frac{\nu^{3/4}\sigma_{\epsilon}}{4(\epsilon)^{5/4}} + \frac{3\sigma_{\nu}}{4(\nu\epsilon)^{1/4}}. \quad (14)$$

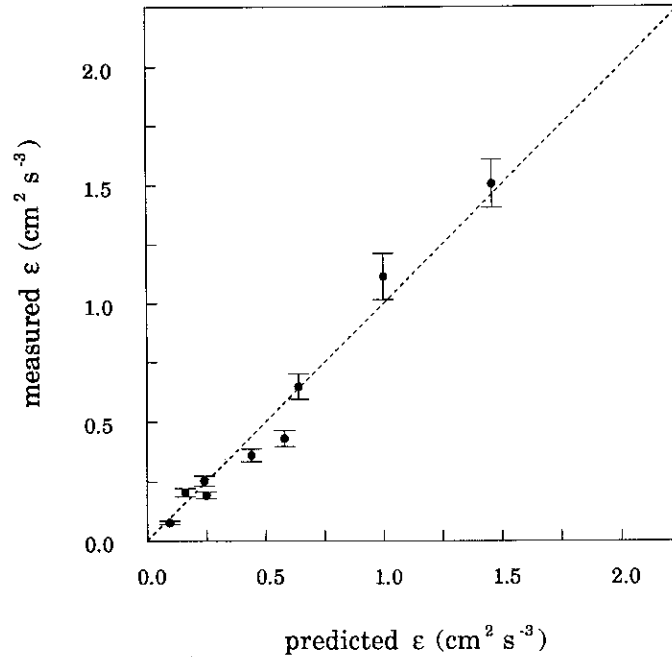


Figure 8. Measured turbulent kinetic energy dissipation rate 20.5 cm from the grid versus dissipation rate predicted from Brumley and Jirka (1987). Error bars represent one standard deviation. Dotted line shows perfect fit to prediction.

The standard deviation in viscosity, σ_ν , is very small (e.g., Fig. 4) so that the second term on the right-hand side of Eq. 14 is negligible.

The magnitude of the fractional error in estimates of (\bar{d}/λ) , taken as $(\sigma_{(d/\lambda)} \lambda/\bar{d})$ was always less than 0.2. Error of this magnitude was substantially smaller than the spread in values of relative velocity-Reynolds number (Fig. 9–10). The disparity in measured error was used to justify the assumption that (\bar{d}/λ) could be treated as an independent variable, and that the relationship between Re and (\bar{d}/λ) could be analyzed appropriately with nonparametric regression analysis that assumes no error in ranking of data along the axis of (\bar{d}/λ) . After plotting the log of Re versus the log of (\bar{d}/λ) , Mood's method of nonparametric linear regression (Tate and Clelland, 1957) was used to test the hypotheses that the data followed expressions for particles smaller than the Kolmogorov scale (Eq. 5) and larger than the Kolmogorov scale (Eq. 4).

4. Results and discussion

Regression analysis yielded similar results for the runs both in salt water, for which (\bar{d}/λ) is greater than one, and the runs in Methocel, for which (\bar{d}/λ) is less than one. At a 95% confidence level the null hypothesis

$$\log Re = 1.33 \log (\bar{d}/\lambda) + \log (1.37) \quad (15)$$

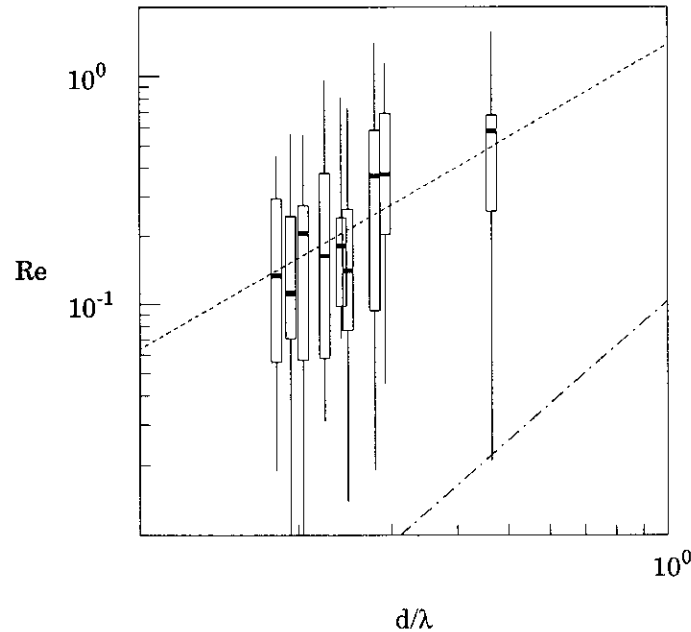


Figure 9. Tukey box plot of relative velocity Reynolds number ($Re = u_r d / \nu$) versus the ratio of mean separation distance, d , to the Kolmogorov scale, $\lambda (= (\nu^3 / \epsilon)^{0.25})$, for runs made in Methocel solution. The thick black lines in each box represent median Re . Box edges mark the 25th and 75th quantiles of Re . Lines extend to minimal and maximal values of Re . The dotted line plots super-Kolmogorov scale theory (Delichatsios and Probstein, 1975) (Eq. 15); the dash-dotted line plots sub-Kolmogorov scale theory (Saffman and Turner, 1956) (Eq. 16).

could not be rejected ($p = 0.077$ for Methocel, $p = 0.091$ for water). The null hypothesis

$$\log Re = 2.00 \log (\bar{d} / \lambda) + \log (0.10) \quad (16)$$

was rejected in both cases ($p = 0.004$) (Fig. 9–10). The data, therefore, support the hypothesis that the encounter rate of particles similar in size to the Kolmogorov scale is controlled by turbulent eddying motions. Viscosity apparently exerts little influence near the Kolmogorov scale. This result directly contradicts recent assertions (not based on data) that viscosity controls the relative velocity of particles for separations as large as ten times the Kolmogorov scale (Lazier and Mann, 1989).

Acceptable ($p > 0.05$) slopes for the Methocel runs are -0.78 – 3.69 . For the runs in NaCl water, the range in slopes is 0.63 – 5.32 . The rejection of sub-Kolmogorov-scale theory therefore arises not from constraint on possible values of the slope in the log-log plots, but rather from a predicted intercept that falls far below values supported by the data. Assuming a slope of 2 based on sub-Kolmogorov-scale theory (Eq. 16), in the Methocel runs 95% confidence limits on the intercept range from

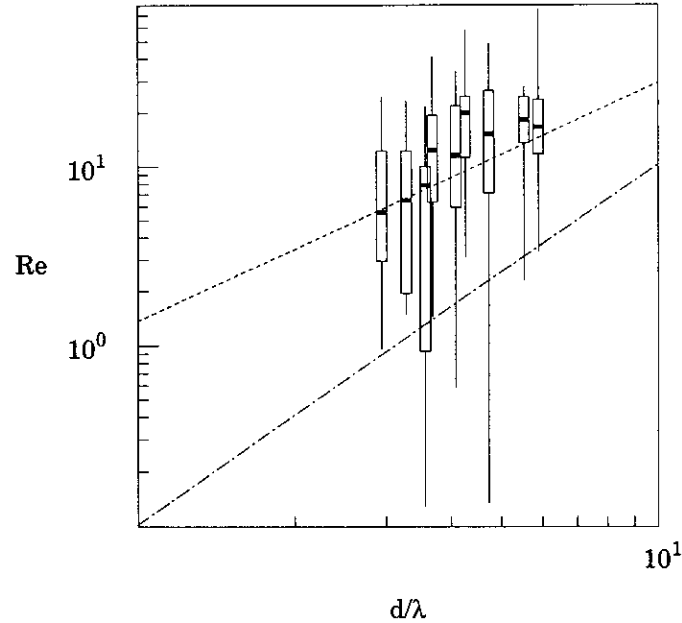


Figure 10. Tukey box plot of Re number versus d/λ for runs made in water. See Figure 9 for explanation.

2.67–4.74, more than an order of magnitude greater than predicted (Eq. 16). Similarly, for the runs in water, an assumed slope of 2 yields 95% confidence limits on the intercept of 0.60–0.92 (Table 6). In contrast, the 95% confidence limits on the intercept when a slope of 1.33 is assumed (Eq. 15) are 1.00–1.93 in the Methocel runs and 1.33–2.19 in the water runs. These values embrace the predicted intercept of 1.37 (Table 6).

Another hypothesis cannot be adequately tested because data from any individual block do not cover the full dynamical range in (d/λ) . It is that at particle sizes similar to the Kolmogorov scale, a plot of $\log Re$ versus $\log (\bar{d}/\lambda)$ should yield a slope greater than 2, thereby joining sub- and super-Kolmogorov-scale theories (Eqs. 15–16). Bearing in mind the qualitative nature of the following observation, it is interesting to note that, if one assumed that the two data sets were from the same experiment, the

Table 6. Ninety-five percent confidence limits on the intercept of $\log Re$ versus $\log (\bar{d}/\lambda)$ plots for assumed slopes of 1.33 and 2.00.

	Slope	Intercept		Theoretical
		Lower limit	Upper limit	
water	1.33	1.33	2.19	1.37
water	2.00	0.60	0.92	0.10
Methocel solution	1.33	1.00	1.93	1.37
Methocel solution	2.00	2.67	4.74	0.10

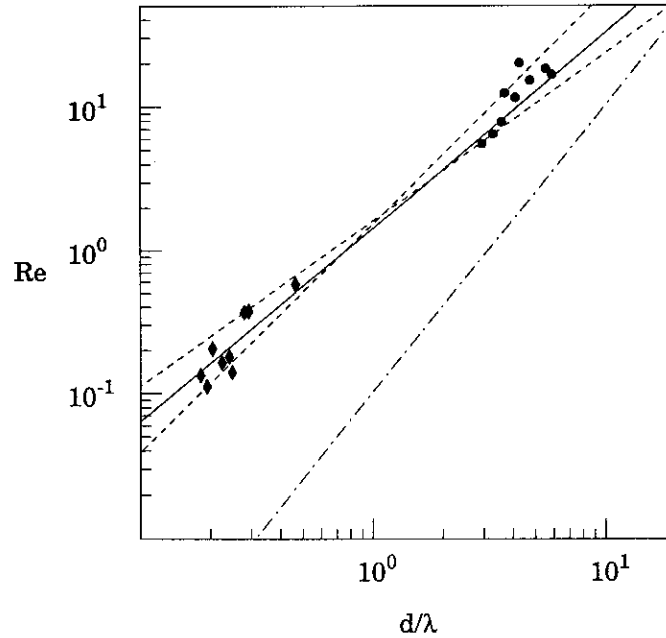


Figure 11. Re versus d/λ for Methocel runs (diamonds) and water runs (circles). The solid line is super-Kolmogorov scale theory (Delichatsios and Probstein, 1975) (Eq. 15); the dotted lines represent maximal and minimal slopes at the 95% confidence level; the dash-dotted line plots sub-Kolmogorov scale theory (Saffman and Turner, 1956) (Eq. 16).

maximal slope one could fit through them is 1.6 (Fig. 11). While this observation cannot be offered as a rejection of the hypothesis that the dynamical region addressed in the experiment is transitional between two inertial regimes, it does favor the hypothesis that fluid inertia dominates interaction of particles at the scales examined in this study.

Several explanations for the success of super-Kolmogorov-scale theory in modeling the relative velocity data exist. First, there may be more turbulent kinetic energy at smaller scales than previously assumed. Second, failure of particles to follow the flow may make them behave effectively as larger particles. Last, the results may represent an artifact arising from the limited separation in turbulent scales in relatively low Reynolds number laboratory tanks.

The poor fit between sub-Kolmogorov-scale theory for particles similar in diameter to the Kolmogorov scale could indicate that the Kolmogorov scale as calculated is actually substantially larger than the smallest eddy size in the fluid. Although there is good evidence that turbulent eddying motions can penetrate to scales smaller than the Kolmogorov scale (Willmarth and Sharma, 1984), numerous studies have shown, on average, a rapid decline in the amount of shear energy at scales smaller than 5–10 times the Kolmogorov scale (e.g., Grant *et al.*, 1962; Oakey and Elliott, 1980).

Numerical simulations also support the sub-Kolmogorov scale relations on which encounter theory is predicated (Balachanadar, 1988). Incorrect treatment of the turbulent kinetic energy budget, therefore, is probably not a viable means of reconciling theory with data.

Several forces that arise from velocity gradients in the undisturbed flow produce relative motion between suspended particles and surrounding fluid. Relative particle-particle velocity is set by the forces responsible for inducing relative motion between neighboring fluid points and by the forces producing relative motion between particles and the fluid. An explicit assumption of particle encounter models is that the forces producing particle-fluid relative velocity are small relative to those producing relative motion between neighboring fluid points (Saffman and Turner, 1956; Delichatsios and Probstein, 1975). Violation of this assumption could limit the responsiveness of particles to high-frequency turbulent fluctuations (Hinze, 1972). Particles responding only to lower frequency fluid motions would behave effectively as larger particles, so that relative particle-particle velocities would reflect larger scale, lower frequency fluid motions than would be expected if the particles acted as passive tracers of the fluid. Alternatively, failure of particles to follow high-frequency fluid motions could result in elevated concentrations of particles in regions of high strain rate (Balachanadar, 1988). Particles similar in diameter to the Kolmogorov scale, therefore, would experience higher shear, on average, than the overall average shear in the fluid.

Scaling arguments are useful for examining the viability of the hypothesis that relative particle-fluid motion is responsible for the success of super-Kolmogorov-scale theory and failure of sub-Kolmogorov-scale theory in matching observed relative particle-particle velocities. The starting point of the scale analysis is the equation of particle motion in terms of the relative particle-fluid velocity, W_i (Maxey and Riley, 1983):

$$\begin{aligned} \left(m_p + \frac{1}{2}m_f\right) \frac{dW_i}{dt} + 6\pi d^2\mu \int_0^t d\tau \frac{dW_i}{d\tau} [\pi\nu(t-\tau)]^{-1/2} + 6\pi d\mu W_i \\ = -m_p \frac{du_i}{dt} + m_f \frac{Du_i}{Dt} + (m_p - m_f)g_i + d^3\pi\mu\nabla^2 u_i \\ + \frac{1}{20} d^2 m_f \frac{d}{dt} (\nabla^2 u_{i|Y(t)}) + \pi\mu d^4 \int_0^t d\tau \frac{d}{d\tau} (\nabla^2 u_{i|Y(t)}) [\pi\nu(t-\tau)]^{-1/2}. \end{aligned} \quad (17)$$

In this equation m_p and m_f are the mass of the particle and of the fluid respectively; d is particle diameter; μ is dynamic viscosity; τ is a time integration variable; t is time; u_i is the undisturbed fluid velocity; d/dt is the time derivative following the particle; D/Dt is the time derivative following a fluid element; g_i is gravitational acceleration; and $Y(t)$ is the position of the center of the particle at time t . The first term of the left-hand side of the equation is the force required to accelerate a particle, including

the added mass effect. The second term is the Basset history term, and the third is Stokes drag. The terms on the right are sources of relative particle-fluid velocity. The first two are particle and fluid inertia, respectively. The third is buoyancy, which may be disregarded in the present context due to the low excess density of the particles. The fourth term represents a correction to Stokes drag that takes account of nonuniform flow on the scale of the particle. Similarly, the last two terms correct the added mass term and the Basset term for nonuniform flow.

Assuming the Kolmogorov length and velocity scales are the relevant scaling parameters (cf. Maxey and Riley, 1983), the following scale estimates of the terms on the right-hand side of Equation 17 emerge:

$$m_p \frac{du_i}{dt} \sim O\left(\frac{d^3 \rho_p (\epsilon \nu)^{1/2}}{\lambda}\right) \quad (18)$$

$$m_f \frac{Du_i}{Dt} \sim O\left(\frac{d^3 \rho (\epsilon \nu)^{1/2}}{\lambda}\right) \quad (19)$$

$$d^3 \pi \mu \nabla^2 u_i \sim O\left(\frac{d^3 \rho \nu^{5/4} \epsilon^{1/4}}{\lambda^2}\right) \quad (20)$$

$$d^2 m_f \frac{d}{dt} (\nabla^2 u_{i|Y(t)}) \sim O\left(\frac{d^5 \rho (\epsilon \nu)^{1/2}}{\lambda^3}\right) \quad (21)$$

$$\pi \mu d^4 \int_0^t d\tau \frac{d}{d\tau} (\nabla^2 u_{i|Y(t)}) [\pi \nu (t - \tau)]^{-1/2} \sim O\left(\frac{d^4 \rho \nu^{7/8} \epsilon^{3/8}}{\lambda^{5/2}}\right). \quad (22)$$

Dividing the scale estimates by the force responsible for inducing relative motion between neighboring fluid points, which is assumed to scale as $\rho(\nu\epsilon)^{1/2}d^2$, yields ratios of the force producing relative particle-fluid motion and the force responsible for relative fluid-fluid motion. This exercise demonstrates that particle and fluid inertia and the Stokes drag term are comparable to the viscous force when (d/λ) is unity. The Basset history term relative to viscous forces goes as $(d/\lambda)^2$, and the added mass term goes as $(d/\lambda)^3$. Particles similar in diameter to the Kolmogorov scale therefore are exposed to a variety of forces that discourage faithful tracking of fluid motions. By examining response times of particles relative to eddy time scales, Hinze (1972) reached a similar conclusion. It is therefore likely that the fit between the data and super-Kolmogorov-scale theory reflects an inability of the particles to follow the flow.

Larger than predicted intercepts on plots of $\log Re$ versus $\log (\bar{d}/\lambda)$ conceivably could be a manifestation of the intrinsic lack in turbulence-tank studies of the degree of separation in scale between energy-producing and energy-dissipating eddies assumed in Kolmogorov's theory of isotropic turbulence (cf. Tennekes and Lumley, 1972). Lack of separation could make the integral length scale of the turbulence, rather than particle separation, the relevant length scale of motion in expressions for particle-particle relative velocity at small scales (Eqs. 3, 5). The maximal effect would

be to increase the intercept by λ/d , which is roughly consistent with measured intercepts (Table 6). However, the dramatic 25-fold difference in viscosity between experiments produces negligible effect in the data, as evidenced by the good fit to data between a line with a slope of 1.33 and the poor fit of a line with a slope of 2 (Fig. 11). The small effect of viscosity change argues against the hypothesis that the results reflect a confounding of eddy scales.

The intrinsic lack of separation in scale between energy-producing and energy-dissipating eddies (cf. Tennekes and Lumley, 1972) calls into question the existence of true inertial subrange in this study. In the absence of an inertial subrange particle-particle relative velocities theoretically are defined by (Delichatsios and Probstein, 1975):

$$u_r = (\epsilon L)^{1/3}, \quad (23)$$

where L is the Eulerian macroscale of the turbulence (Tennekes and Lumley, 1972). In nondimensional form,

$$Re = (L/d)^{1/3}(d/\lambda)^{4/3}. \quad (24)$$

This equation differs from Eq. 7 only in the leading coefficient. If L is roughly equal to the grid spacing (6.35 cm) then the leading coefficient is roughly equal to 3. It would be difficult, therefore, to distinguish whether particles were responding to eddies in the inertial subrange or, in the absence of an inertial subrange, to larger scale eddies. This issue is not of practical importance because the central question of the study is whether the relative velocities of particles similar in diameter to the Kolmogorov scale are governed by viscosity. Clearly they are not.

Presumably, at some small (<0.2) value of (\bar{d}/λ) , viscosity must control the relative velocity between closely spaced particles, so that the slope of a $\log Re$ versus $\log(\bar{d}/\lambda)$ plot is two. The value of (\bar{d}/λ) at which the transition to a viscosity-dominated regime occurs and the functional form of the transition are unclear. Two possibilities exist for how $\log Re$ is related to $\log(\bar{d}/\lambda)$ at transitional values of (\bar{d}/λ) . The first, already discussed, is that at some unspecified relative particle size, the slope of a $\log Re$ versus $\log(\bar{d}/\lambda)$ plot steepens to greater than two. The line eventually intersects one of the proposed sub-Kolmogorov-scale lines (e.g., Eq. 16). The second is that at some unspecified relative particle size, the slope of a $\log Re$ versus $\log(\bar{d}/\lambda)$ plot steepens to a value of two and maintains an intercept substantially greater than predicted. Given the preceding arguments, it is most likely that as particle size becomes much smaller than the Kolmogorov scale, relative velocities converge to one of the sub-Kolmogorov-scale expressions. Either scenario suggests that the ratio of actual to predicted relative particle velocity at small scales (e.g., $(\bar{d}/\lambda) \leq 0.1$) may exceed unity for a large range of relative particle sizes.

Previous studies aimed at estimating relative velocities between particles smaller than the Kolmogorov scale suffer from a shared, indirect approach that both

precludes comparison with the results here and limits the value of their results for estimating encounter rates of small ($\ll \lambda$) particles. In these studies estimates of relative velocity derive from changes in particle number density N (Eq. 1) as a function of time in a turbulent fluid (Birkner and Morgan, 1968; Argaman and Kaufman, 1970; Delichatsios and Probststein, 1975). Results from this inverse method are sensitive to model assumptions. For example, failure to account for multiple particle sizes that are present either initially or because of aggregation can bias results significantly (Delichatsios and Probststein, 1975). Depositional losses to vessel walls confound estimates of encounter rate. In the most careful study to date (Delichatsios and Probststein, 1975), conservatively low estimates of deposition to the pipe walls, calculated with the method of Davies (1966), show that deposition rate is of the same magnitude as aggregation rate and that depositional losses could substantially alter the time rate of evolution of particle number density. Complex particle-particle interactions make separation of the process of encounter from the poorly constrained process of particle contact (e.g., Hill, 1992) impossible. Last, particle breakup is not included and may exert a strong influence on the time evolution of particle number density (e.g., Birkner and Morgan, 1968). Resolution of encounter rates for sub-Kolmogorov-scale particles awaits direct measurements of relative velocities.

In any case, our data provide clear evidence that relative velocity between neighboring particles induced by turbulent shear for (\bar{d}/λ) values of 0.2–6.0 exceed velocities previously assumed for this range (Delichatsios and Probststein, 1975; Lazier and Mann, 1989; Hill, 1992) by 4–40 times. These (\bar{d}/λ) values translate to particles sizes of ≈ 0.01 –1.0 cm in the surface ocean. Underprediction of relative velocity would result in low estimates of aggregation rate of large particles by turbulent shear. Larger-than-predicted rates of physical aggregation lend support to the hypothesis that physical aggregation can bring about the repackaging of small, slowly sinking particles into large, rapidly sinking aggregates required by observations of high vertical fluxes in the sea (e.g., Smetacek, 1985). Predicated on a large body of field data, the hypothesis has been questioned because of difficulty in reconciling predicted physical aggregation rates with rates inferred from vertical fluxes (McCave, 1984; Hill, 1992). Hill (1992) proposed that underestimation of turbulent-shear aggregation rates was a possible source of difficulty. The data here support this proposition.

These data also hold implications for the encounter rate between organisms and between organisms and nutrient patches in the sea. Previously, when calculating passive, physical encounter rates between predator and prey, the steepening decline in relative velocity between neighboring particles associated with transition to a viscosity-dominated regime has been assumed to occur at relatively large scales (e.g., $(\bar{d}/\lambda) > 6$ (Rothschild and Osborn, 1988; Lazier and Mann, 1989)). The results here suggest that relative velocity remains high to substantially smaller scales. Therefore,

the potential for turbulence to enhance encounter rates dramatically (Rothschild and Osborn, 1988) extends to smaller scales than previously supposed, a possibility discussed by Shimeta and Jumars (1991).

Encounter of bacteria and phytoplankton with microscale nutrient patches typically takes place on smaller scales (< 0.01 cm) than those addressed in this study (e.g., Mitchell *et al.*, 1985). The results hint that relative velocities even on these small scales may be much larger than predicted using Eq. 3 or Eq. 5. Nutrient shells about plankton, however, are deformable, and therefore are much more likely to track fluid motions. As a result, one would not expect encounter rates higher than predicted by sub-Kolmogorov-scale theory, presuming this theory to be sound for small particles able to track fluid motions.

5. Conclusion

The first direct measurements of relative velocities between spheres separated by a distance roughly equal to the Kolmogorov scale, when compared with estimates of turbulent kinetic energy dissipation rate, reveal that turbulent-eddy motions control the relative velocity between particles. Adherence to super-Kolmogorov-scale theory around the Kolmogorov scale fits the data and yields relative velocities substantially greater than predicted by assuming that sub-Kolmogorov-scale theory is correct at this scale, as has been done in the past. The success of super-Kolmogorov-scale theory is apparently a manifestation of the effect that particle size has in limiting the ability of particles larger than roughly one-tenth the Kolmogorov scale to follow high-frequency fluid motions. Perhaps the filtering by particles of high-frequency motions makes particles behave effectively as larger particles, responding only to super-Kolmogorov-scale eddies. Alternatively, failure of particles to follow high-frequency fluid motions may result in accumulation of particles similar in diameter to the Kolmogorov scale in high-strain-rate regions of the fluid. In either case higher relative velocities produce higher aggregation rates by turbulent shear of large particles and higher predator-prey contact rates. The results suggest that past calculations of encounter rates of particles and organisms have been biased towards biological mechanisms of encounter and away from physical mechanisms.

The next critical step in improving understanding of the role of small-scale turbulence in oceanic biogeochemical cycles is elucidation of relative velocities between particles much smaller than Kolmogorov scale. The data here provide reason to question the range of applicability and accuracy of expressions for relative velocity at these small scales. Effects of turbulence may extend to scales much smaller than previously imagined.

Acknowledgments. We thank B. Bruner, J. Nelson, R. Shreeve, and D. Thoreson for invaluable technical assistance. Thanks also go to B. Dade, J. Riley and K. Stolzenbach for comments on earlier versions of the manuscript. This work was supported by ONR contract

N00014-90-J-1078 to A. Nowell and P. Jumars. Contribution no. 1949 from the University of Washington.

REFERENCES

- Argaman, Y. and W. J. Kaufman. 1970. Turbulence and flocculation. *J. Sanit. Engr. Div., ASCE*, 96(SA2), 223–241.
- Bacon, M. P., C.-A. Huh, A. P. Fleer and W. G. Deuser. 1985. Seasonality in the flux of natural radionuclides and plutonium in the deep Sargasso Sea. *Deep-Sea Res.*, 32, 273–286.
- Balachandrar, S. 1988. Particle coagulation in homogeneous turbulence. Ph.D. dissertation, Brown University, 149 pp.
- Birkner, F. B. and J. J. Morgan. 1968. Polymer flocculation kinetics of dilute colloidal suspensions. *J. Am. Water Works Assn.*, 60, 175–191.
- Brumley, B. H. and G. H. Jirka. 1987. Near-surface turbulence in a grid-stirred tank. *J. Fluid Mech.*, 183, 235–263.
- Conover, W. J. 1980. *Practical Nonparametric Statistics*. John Wiley & Sons, Inc., New York, 493 pp.
- Davies, C. N. 1966. Deposition from moving aerosols, in *Aerosol Science*, C. N. Davies, ed., Academic Press, NY, 393–446.
- Delichatsios, M. A. and R. F. Probstein. 1975. Coagulation in turbulent flow: Theory and experiment. *J. Colloid Interface Sci.*, 51, 394–405.
- Grant, H. L., R. W. Stewart and A. Moillet. 1962. Turbulence spectra from a tidal channel. *J. Fluid Mech.*, 12, 241–268.
- Hill, P. S. 1992. Reconciling aggregation theory with observed vertical fluxes following phytoplankton blooms. *J. Geophys. Res.*, 92(C2), 2295–2308.
- Hinze, J. O. 1972. Turbulent fluid and particle interaction, in *Progress in Heat and Mass Transfer*, 6, G. Hetsroni, S. Sideman and J. P. Hartnett, eds., Pergamon Press, Oxford, 433–452.
- Honjo, S. 1982. Seasonality and interaction of biogenic and lithogenic particulate flux at the Panama Basin. *Science*, 218, 883–884.
- Landau, L. D. and E. M. Lifshitz. 1959. *Fluid Mechanics*. Pergamon Press, Reading, MA, 536 pp.
- Lazier, J. R. N. and K. H. Mann. 1989. Turbulence and the diffusive layers around small organisms. *Deep-Sea Res.*, 36, 1721–1733.
- Maxey, M. R. and J. J. Riley. 1983. Equation of motion for a small rigid sphere in a nonuniform flow. *Phys. Fluids*, 26, 883–889.
- McCave, I. N. 1984. Size spectra and aggregation of suspended particles in the deep ocean. *Deep-Sea Res.*, 31, 329–352.
- Mitchell, J. G., A. Okubo and J. A. Fuhrman. 1985. Microzones surrounding phytoplankton form the basis for a stratified marine microbial ecosystem. *Nature*, 316, 58–59.
- Oakey, N. S. and J. A. Elliott. 1980. Dissipation in the mixed layer near Emerald Basin, in *Marine Turbulence*, J. C. J. Nihoul, ed., Elsevier, Amsterdam, 123–133.
- Rothschild, B. J. and T. R. Osborn. 1988. Small-scale turbulence and plankton contact rates. *J. Plank. Res.*, 10, 465–474.
- Saffman, P. G. and J. S. Turner. 1956. On the collision of drops in turbulent clouds. *J. Fluid Mech.*, 1, 16–30.
- Sheldon, R. W., A. Prakash and W. H. Sutcliffe, Jr. 1972. The size distribution of particles in the ocean. *Limnol. Oceanogr.*, 17, 327–340.

- Shimeta, J. and P. A. Jumars. 1991. Physical mechanisms and rates of particle capture by suspension-feeders. *Oceanogr. Mar. Biol. Annu. Rev.*, 29, 191–257.
- Smetacek, V. S. 1985. Role of sinking in diatom life-history cycles: Ecological, evolutionary and geological significance. *Mar. Biol.*, 84, 239–251.
- Smith, D. M. and D. M. Meadows. 1974. Power spectra from random-time samples for turbulence measurements with a laser velocimeter, *in* Proceedings of the Second International Workshop on Laser Velocimetry, 2, H. D. Thompson and W. H. Stevenson, eds., Engineering Experiment Station, *Bulletin 144*, Purdue University, W. Lafayette, IN, 27–46.
- Smoluchowski, M. 1917. Versuch einer mathematischen Theorie der Koagulationskinetik kolloider Lösungen. *Z. Phys. Chem.*, 92, 129–168.
- Tate, M. W. and R. C. Clelland. 1957. *Nonparametric and Shortcut Statistics*. Interstate Printers and Publishers, Inc., Danville, IL, 171 pp.
- Taylor, J. R. 1982. *An Introduction to Error Analysis: The Study of Uncertainties in Physical Measurements*. University Science Books, Oxford University Press, Mill Valley, CA, 300 pp.
- Tennekes, H. and J. L. Lumley. 1972. *A First Course in Turbulence*. The MIT Press, Cambridge, MA, 293 pp.
- van Leussen, W. 1988. Aggregation of particles, settling velocity of mud flocs: a review, *in* Physical Processes in Estuaries, J. Dronkers and W. van Leussen, eds., Springer-Verlag, NY, 348–403.
- Veth, C. 1983. Turbulence measurements in the stratified central North Sea with laser-doppler velocimeter system, *in* North Sea Dynamics. J. Sündermann and W. Lenz, eds., Springer-Verlag, Berlin, 412–428.
- Willmarth, W. W. and L. K. Sharma. 1984. Study of turbulent structure with hot wires smaller than the viscous length. *J. Fluid Mech.*, 142, 121–149.
- Yamazaki, H. and T. R. Osborn. 1988. Review of oceanic turbulence: implications for biodynamics, *in* Toward a Theory on Biological-Physical Interactions in the World Ocean. B. J. Rothschild, ed., Kluwer Academic Publishers, 215–234.